

**Analysis of trends in momentum multiplication factor predictions and uncertainties in the DART mission**  
Sung Wook Paek<sup>(1)</sup>, Olivier de Weck<sup>(2)</sup>

<sup>(1)</sup>City, University of London  
London, United Kingdom  
Email:sung.paek@city.ac.uk

<sup>(2)</sup>Massachusetts Institute of Technology  
Cambridge, United States  
Email:deweck@mit.edu

**Abstract – Hypervelocity experiments, started as regolith formation studies, also came to be applied in planetary defence. The efficacy of asteroid deflection is measured in terms of momentum multiplication factor ( $\beta$ ) and was measured in the Double Asteroid Redirection Test (DART) for the first time. The estimation trends of  $\beta$  and additional uncertainties to consider in the DART mission are presented.**

### I. INTRODUCTION

The Double Asteroid Redirection Test (DART) on September 26, 2022, marked humanity’s first demonstration of purposefully changing the motion of a celestial object. The altered orbit of Dimorphos’s orbit around Didymos has a new period of 11 hours, 22 minutes, and 3 seconds, shortened by 33 minutes and 15 seconds from the original period before deflection. This outcome exceeds the minimum success criterion by NASA, defined as a period change of 73 seconds, by more than 25 times. Although the test was carried out within the binary system of Didymos (primary) and Dimorphos (secondary), the same kinetic-impact (KI) technique can be extended to a planetary defence scale. In this unlikely but critical event, the heliocentric velocity of a potentially hazardous object would be changed. The objective of this paper is to provide a short review of how the previous estimates changed in the momentum enhancement properties of Dimorphos, along with underlying assumptions.

### II. DART MISSION BACKGROUND AND OUTCOMES

65803 Didymos (1996 GT) is a sub-kilometre, Apollo-group asteroid whose perihelion is greater than Earth’s aphelion. Its moon, Dimorphos, was discovered in 2003. Binary asteroid systems provide advantages in terms of KI testing because the secondary’s motion can be tracked via light curve measurements on the ground. Furthermore, the delta-v to rendezvous with Didymos is among the lowest (5.1 km/s) and the secondary is not too massive compared to the primary, which made the binary mission affordable to carry out and its outcomes measurable. Table 1 summarises the gravimetric properties of the binary system.

Table 1. Gravimetric properties of Didymos and Dimorphos

	properties	
	value	unit
Didymos (1) mass	$5.2 \times 10^{11}$	kg
Dimorphos (2) volume	0.00174	km <sup>3</sup>
Dimorphos (2) mass	$5 \times 10^9$	kg
System GM (1+2)	$35.4 \pm 1.5$	m <sup>3</sup> s <sup>-2</sup>
Didymos (1) diameter	$765 \pm 15^*$	m
Dimorphos (2) diameter	$164 \pm 18^{**}$ $153 \pm 2^{***}$	m

\*Cheng (2022)[2], \*\*Rivkin (2021)[1], \*\*\*Daly (2023) [3]

In addition to decreasing Dimorphos’s orbital period around Didymos, the DART impact also led to an instantaneous reduction in Dimorphos’s along-track velocity, approximately 2.70 mm/s [3]. The mean orbital distance between Dimorphos and Didymos has been shortened to 1,152 meters, 37 meters closer than before the impact. The impact velocity components are  $U_x = 3.574$  km/s,  $U_y = -4.641$  km/s, and  $U_z = -1.856$  km/s at the impact time of September 26, 2022, 23:14:24.183 UTC using the Earth Mean Equator J2000 (EME J2000) coordinate frame, as depicted in Fig. 1. Using the local Dimorphos-centred frame, the same impact velocity may be represented as  $U'_x = -1.06$  km/s,  $U'_y = 5.96$  km/s, and  $U'_z = 1.03$  km/s; panels (a) and (b) of Fig. 2 define the coordinate axes and indicate the impact location where the DART spacecraft collided with Dimorphos.

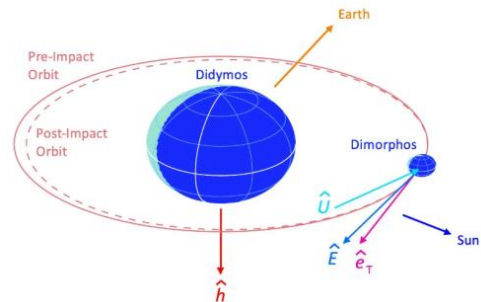


Fig. 1. Velocity vectors during DART impact [4].

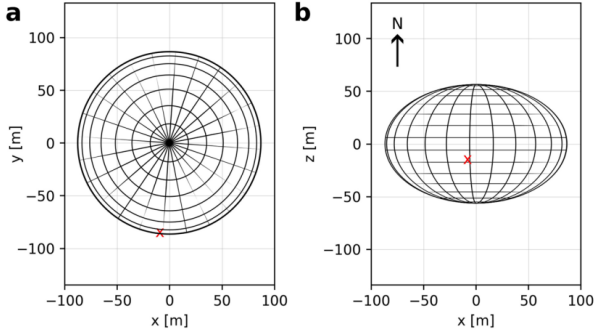


Fig. 2. DART impact location in Dimorphos local coordinates [4]: (a) Top view (b) Side view.

The latest observation data suggests that DART impact has also substantially altered Dimorphos's shape from an oblate spheroid to a rather ellipsoidal shape (Naidu, 2024). In other words, the asteroid was shaped like a squashed ball before impact whereas it currently resembles a rugby ball as depicted in Fig. 3 [5]. The equatorial axis ratios could be as large as 1.3 and 1.6 in the equatorial plane of post-impact ellipsoid, which is to be finalised through a follow-up mission in 2026 [6, 7]. It should be noted that the complete knowledge of the pre-impact shape is no longer available after permanent deformation. In-situ measurements were carried out by LICIACube (Light Italian CubeSat for Imaging of Asteroids), released from the DART spacecraft 15 days before impact, but its coverage was limited because it performed a fly-by instead of orbiting around the binary system.

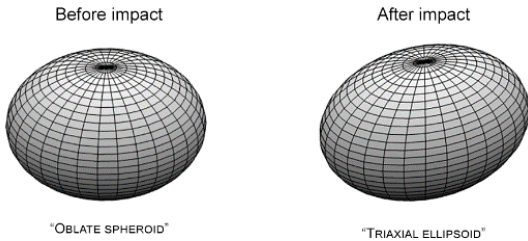


Fig. 3. Dimorphos shape change before and after DART impact [5].

The momentum transfer process can be expressed as (1), where the net momentum is conserved before (left) and after (right) the impact:

$$M\Delta v = m\mathbf{U} + m(\beta - 1)(\hat{\mathbf{E}} \cdot \mathbf{U})\hat{\mathbf{E}} \quad (1)$$

On the left-hand side,  $M$  is the Dimorphos mass,  $\Delta v$  is the impact-induced change in Dimorphos's orbital velocity, and thus  $M\Delta v$  is the momentum transferred to Dimorphos. On the right-hand side,  $m$  is the DART spacecraft mass at impact (579.4 kg),  $\mathbf{U}$  is DART's velocity relative to Dimorphos at impact, and the

product  $m\mathbf{U}$  is DART's incident momentum. In the last term,  $\hat{\mathbf{E}}$  is the direction vector for net ejecta momentum, whose components were estimated from DART measurements ( $E_x^{\hat{}}=-0.7241$ ,  $E_y^{\hat{}}=0.6520$ ,  $E_z^{\hat{}}=0.2250$ ); the product term  $(\beta-1)(\hat{\mathbf{E}} \cdot m\mathbf{U})\hat{\mathbf{E}}$  is ejecta's net momentum written in terms of  $m\mathbf{U}$ . Called either momentum multiplication factor or momentum enhancement factor,  $\beta$  is a measure of the efficiency of deflection following a kinetic impact. Equation (2) is obtained, as below, by solving (1) for  $\beta$  after introducing an along-track unit vector  $\hat{\mathbf{e}}_T$ . The definition of  $\beta$  in (2) is based on the impactor's momentum projected onto the net ejecta momentum. The value might change slightly if the projection is onto the spacecraft's velocity.

$$\beta = 1 + \frac{\frac{M}{m}(\Delta v \cdot \hat{\mathbf{e}}_T) - (\mathbf{U} \cdot \hat{\mathbf{e}}_T)}{(\hat{\mathbf{E}} \cdot \mathbf{U})(\hat{\mathbf{E}} \cdot \hat{\mathbf{e}}_T)} \quad (2)$$

### III. COMPARISON WITH LITERATURE AND PRIOR ESTIMATES

Hypervelocity impact experiments date back to the 1960s when researchers studied the cratering process on lunar/planetary surfaces [8]. Since then, noncohesive quartz sand has been used as a target medium to emulate lunar regolith formation [9]. Experiments using impact velocities up to 7 km/s for regolith-like targets resulted in  $\beta$  values ranging from 1.5 to 2.25 [10]. As the characterization of ejecta velocity distributions became possible, accumulation of measurement data led to the development/refinement of scaling laws and ejecta models [11]. In particular, the dependence of ejecta velocity distribution on impactor characteristics has become relatively well-characterised [12]; Fig. 4 illustrates some target variables that affect the creation of a crater and debris ejected from it. Computer simulations, cross-verified with projectile experiments, yielded  $\beta$  values of 1 to 2 for target cohesion strengths of a few MPa, according to Holsapple and Housen (2012) [12], Jutzi and Michel (2014) [13], and Stickle et al. (2015). Narrower ranges were suggested, such as 1.28-1.39 (Stickle et al., 2017 [14]) and 1.5-2 (Rainey et al., 2020 [15]), after incorporating the DART parameters. Sensitivity analyses were also carried out on the target strength parameters, amongst which target porosity, yield strength (low pressure), tensile strength,

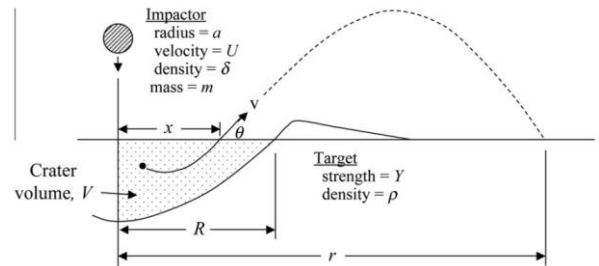


Fig. 4. Variables of impactor and target characteristics [12].

crack spacing, and internal friction coefficient had the highest statistical significance for predicting  $\beta$ . Higher  $\beta$  ranges were reported from small-scale experiments (3-4) with nearly non-porous quartzite, river rock, or carbonaceous chondrite samples [16]. Similar results were obtained for high-porosity targets ( $\sim 20\%$ ) if the following conditions are satisfied [17]:

- the samples are hydrous enough to eject water vapor upon impact
- the cohesive strength is very low, as seen in weak sand/rock targets ( $\sim 1\text{kPa}$ ).

Computer simulations enabled the testing of low-cohesive-strength cases, whose loose structure (rubble pile) is difficult to physically re-enact in reality. The lower-end cohesion strengths of hundreds or tens of Pa led to  $\beta$  values up to 5, delineated as a parallel plot in Fig. 5, where porosity and internal friction coefficient also have significant effects [18]. The coefficient of internal friction is derived from the Mohr–Coulomb yield surface, which is a theory to model the cohesive-frictional materials. An increase in coefficient of friction or cohesive strength will decrease the crater volume and ejecta mass, thus increasing  $\beta$  [19].

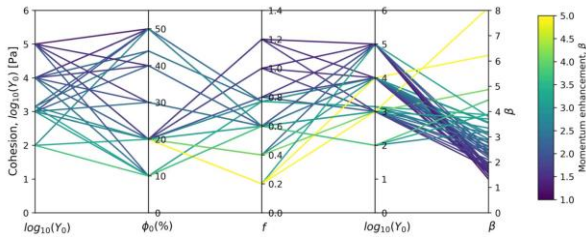


Fig. 5. Interaction and ranges of initial porosity ( $\phi_0$ ) and material strength parameters (coefficient of internal friction  $f$  and cohesion strength  $Y_0$ ) [18].

The  $\beta$  predictions before DART were speculative since the structural properties of Dimorphos are largely unknown. The uncertainty in the binary systems’s GM product is further propagated into the interactions of mass, volume, density and porosity containing uncertainty. Dimorphos’s porosity was assumed to be 20% using a density of  $2170 \pm 350 \text{ kg/m}^3$  (Ferrari, 2022 [20]), and dynamical consideration suggested the cohesive strength around 10 Pa, which altogether led to a  $\beta$  value of 4 from Fig. 6 [18]. This seems close to the mean  $\beta$  value of 3.61 from DART data measurements assuming a density of  $2400 \text{ kg/m}^3$ [2]. The  $1\sigma$  range for  $\beta$  is [3.36, 3.80], around the mean of 3.61, and the mean value of changes from 2.2 to 4.9 across the density range from  $1500 \text{ kg/m}^3$  to  $3300 \text{ kg/m}^3$ , as depicted in Fig. 7 [2]. Reference [18] may still be argued as over-estimation because the data fit formula in Fig. 7 gives a  $\beta$  value of 3.26 for the density of  $2170 \text{ kg/m}^3$ ; the coordinate location of  $(2170 \text{ kg/m}^3, 4)$  is clearly outside the  $3\sigma$  band shown in Fig. 7.

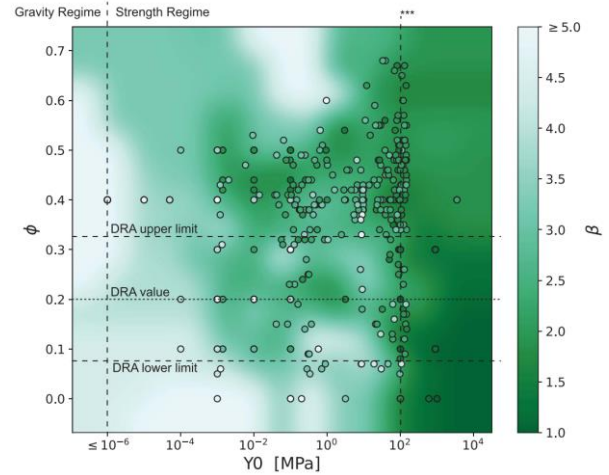


Fig. 6. The dependence of  $\beta$  on target porosity ( $\phi_0$ ) and yield strength (cohesion,  $Y_0$ ), with Design Reference Asteroid (DRA) limits [18] (\*\*\*: [21]).

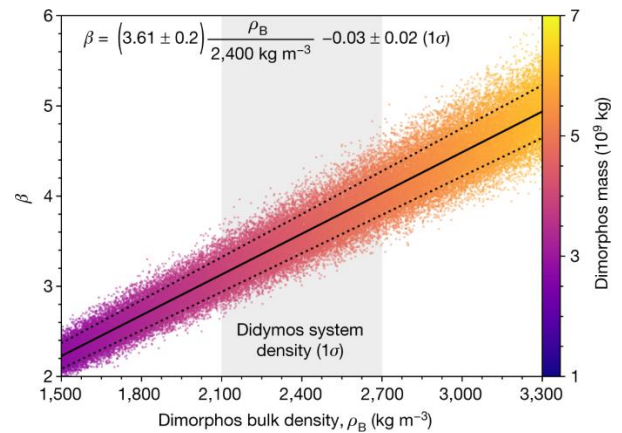


Fig. 7. The linear fit of mean  $\beta$  values across the  $3\sigma$  range of Dimorphos bulk density (among which  $3\sigma$  range is shaded) [2].

Planned to be launched in October 2024, European Space Agency’s Hera project aims at surveying Dimorphos to characterise its mass and structure while quantifying the effect of DART impact. The dimensions and morphology of the crater and the ejecta cloud could be scrutinised when the Hera spacecraft arrives at the binary system in 2026. Reference [2] and its results summarised in Fig. 7 will be updated once the Dimorphos density is determined within a few-percent error range, as was done in asteroid proximity missions to 25143 Itokawa and 101955 Benu.

#### IV. POSSIBLE FACTORS CONTRIBUTING TO UNCERTAINTIES AND ERRORS

The previous section briefly reviewed the estimates of momentum enhancement factor for the DART impact. After the results in Fig. 7 became available, [4] proposed the following candidate solutions that best match the  $\beta$  value from [2]:

- bulk density of 2360 kg/m<sup>3</sup> (grain density of 3500 kg/m<sup>3</sup>, boulder packing 30 vol%), internal friction coefficient of 0.4, and cohesive strength less than 10 Pa.
- bulk density of 2160 kg/m<sup>3</sup> (grain density of 3200 kg/m<sup>3</sup>, boulder packing 30 vol%), internal friction coefficient of 0.4, and cohesive strength of around or less than 2 Pa.

- Escape velocity from Dimorphos's surface : 8.92 cm/s (two-body problem between Dimorphos and ejecta).
- Mean orbital speed of Dimorphos : 17.3 cm/s
- Escape velocity from the binary system at 1.18 km (mean orbital distance between primary and secondary) from the barycenter: 24.4 cm/s.
- Escape velocity from Didymos's surface: 42.3 cm/s

The second set of conditions indicates that the inter-boulder medium (matrix) is almost cohesionless. Apart from these two end-members, the other simulations all resulted in  $\beta$  values less than 3.61. Considering the restricted nature of these combinations, there is a possibility of underestimation if the actual parameters of Dimorphos do not exactly match the prescribed (estimated) conditions.

For example, ejecta with  $\sim 8.9$  cm/s velocities will be re-accreted by Dimorphos, ejecta with  $\sim 50$  cm/s will tend to escape the binary system or be accreted on the primary according to the above. Debris with moderate values might be trapped into orbits in the binary system temporarily and settle down to various end states. For momentum enhancement to happen, ejecta must lift off Dimorphos's surface and escape its gravity well. If Dimorphos were by itself, not bound by Didymos and not influenced by the Sun, a simple two-body dynamics would govern the dynamics between Dimorphos and ejecta. However, the existence of the primary (Didymos) reduces the required speed of debris to eject the gravitational influence of Dimorphos. Ferrari and Lavagna calculated the minimum escape speed on the order of  $\sim 4.5$  cm/s (escape through L1 of the Didymos–Dimorphos system) and  $\sim 5.1$  cm/s (escape through L2). It should be noted that these numbers correspond to the rather ideal scenarios when the ejecta follows the minimum delta-v manifold trajectory. According to simulations summarised in Fig. 9, some of the debris above 5 cm/s will re-impact Dimorphos (blue) instead of co-orbiting Didymos (black) or escaping the binary system (magenta).

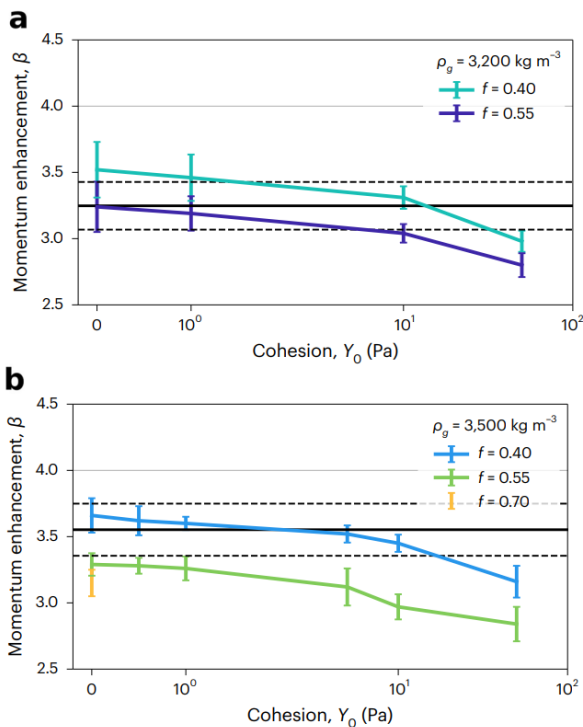


Fig. 8. (a)  $\beta$  as a function of target matrix cohesion ( $Y_0$ ) for the DART impact with varying coefficient of internal friction ( $f=0.40$  or  $0.55$ ) with fixed grain density  $\rho_g = 3,200$  kg/m<sup>3</sup> and 30 vol% boulder packing (horizontal lines from bulk density  $\rho_B = 2,160$  kg m<sup>-3</sup>) (b)  $\beta$  for  $f=0.40, 0.55, 0.70$ ,  $\rho_g = 3,500$  kg/m<sup>3</sup> and 30 vol% boulder packing (horizontal lines from  $\rho_B = 2,160$  kg m<sup>-3</sup>) [2].

In principle,  $\beta$  is determined from how the spacecraft's injection momentum is allocated between the target and the ejecta cloud. Because the target of impact is a secondary of a binary system in the case of DART, the primary may attract some ejecta of the debris cloud and the following (escape) velocities should be considered [22]:

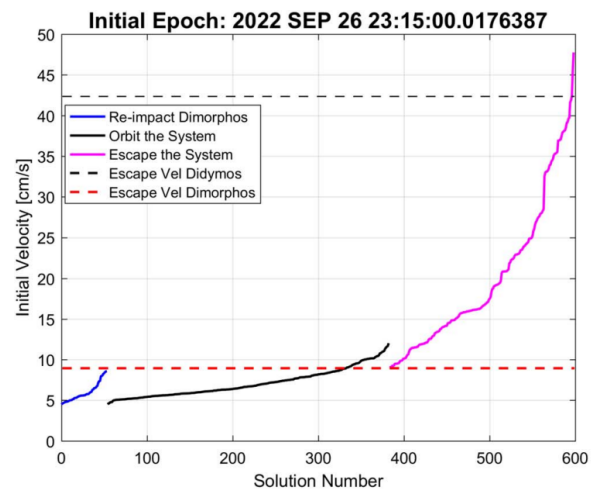


Fig. 9. The ejecta speed profile at DART's impact [20]

Possible under-estimation of [2] could be explained by the following contributing factors that might boost  $\beta$  by turning some proportion of re-impacting debris into the co-orbiting or escaping group.



### A. Third-body perturbation

The gravitational influence of Didymos on Dimorphos is listed in Table 2 in terms of acceleration and Lagrange point (L1) position, which nearly halved the minimum escape speed as mentioned before. The gravitational acceleration of the Sun would take debris further away, if the debris managed to escape the influence of the binary system where the asteroids' gravitational forces dominate (few km within Didymos), as shown in Fig. 10. The figure plots perturbing acceleration values, which is much smaller than those in Table 2 because the change in escape speeds by a third body arises from relative acceleration. The perturbation is proportional to the vector difference of the nearly same two vectors, the ejecta-3<sup>rd</sup> body vector and the asteroid-3<sup>rd</sup> body vector. The mean tidal acceleration from the Sun is on the order of  $10^{-10}$  m/s<sup>2</sup> at 10 km distance in Fig. 10, and that from Earth is on the order of  $10^{-12}$  m/s<sup>2</sup> at the same distance. The geometrical alignment of the Didymos system, the Sun, and Earth, their escape-speed-reducing effects could add up but would be still minimal in extent. The Earth's contribution in perturbing forces would be larger if the asteroid system were closer at spacecraft impact, on the order of  $10^6$  km.

Table 2. Binary system environment.

pairs	Dynamic properties	
(A around B)	Gravitational Acceleration (by B)	L1 location (from A)
Dimorphos - Didymos	$2.49 \times 10^{-5}$ m/s <sup>2</sup>	0.17 km
Didymos - Earth	$3.12 \times 10^{-6}$ m/s <sup>2*</sup>	374 km
	$3.54 \times 10^{-6}$ m/s <sup>2**</sup>	325 km
Didymos - Sun	0.0056 m/s <sup>2</sup>	68 km

\* $1.13 \times 10^7$  km on 22 Sep 2022

\*\* $1.06 \times 10^7$  km on 4 October 2022

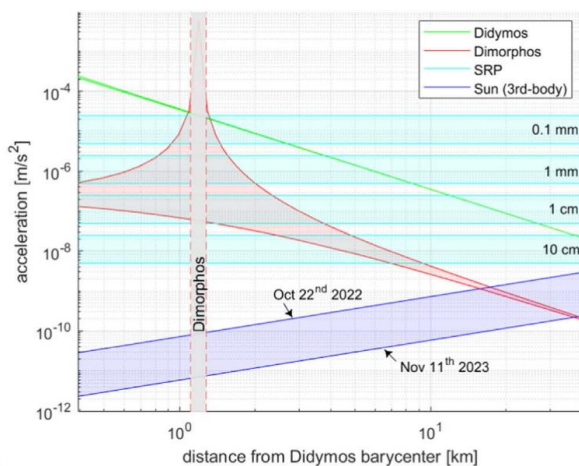


Fig. 10. Accelerations affecting the ejecta motion near Didymos [20].

### B. Solar radiation

Solar radiation pressure (SRP) is an exchange in momenta between the photons emitted by the Sun and the surface of an object. The SRP values are shown for different ejecta sizes where smaller particles drift faster away from the asteroid due to higher area-to-mass ratios. Depending on the cases, SRP accelerations can be as large as asteroid accelerations; therefore, the size distribution, as well as the morphology and albedo (reflectivity) characteristics of the ejecta may have moderate influences on  $\beta$ . The eclipses by the binary asteroids may have minor effects on SRP experienced by the ejecta particles, affecting  $\beta$ . The variation of SRP from solar maxima to solar minima (electromagnetic) and the variation of solar wind pressure (plasma) are minimal, on the order of  $\sim 0.1\%$ .

### C. Energy released from spacecraft

Past research showed that spacecraft geometry or impact orientation does not affect  $\beta$  notably in the long term. However, little attention has been given to the effect of energy released from the spacecraft's remaining fuel, pressurised tank, or onboard batteries in conjunction with hypervelocity. Currently, there is no satellite breakup model to describe the combined effect of impact and explosion; NASA's standard breakup model provides separate delta-v distributions for collision and explosion cases [23]. It remains difficult, therefore, to assess the kinetic-chemical combined effects on the ejecta characteristics and eventually the  $\beta$  value.

## V. CONCLUSION

The estimation of momentum enhancement factor  $\beta$  has been speculative, but the DART mission has advanced our understanding of rubble-pile asteroids significantly. The follow-up Hera mission will unveil some of the uncertain variables, which will further refine our model of the asteroid system and dynamical process it went through. Some uncertainty factors suggested here might be worth investigating to identify biases, if any, in the best available estimates. Bridging the gap between small-scale ground experiments and large-scale missions would be useful in devising reliable asteroid deflection strategies [24].

## VI. REFERENCES

- [1] A.S. Rivkin, N.L. Chabot, A.M. Stickle, C.A. Thomas, D.C. Richardson, O.S. Barnouin, E.G. Fahnestock, C.M. Ernst, A.F. Cheng, S. Chesley, and S. Naidu. "The Double Asteroid Redirection Test (DART): planetary defense investigations and requirements," *The Planetary Science Journal*, vol. 2, no. 5, p. 173, August 2021.
- [2] A.F. Cheng, H.F. Agrusa and B.W. Barbee, A.J. Meyer, T.L. Farnham, S.D. Raducan, D.C. Richardson, E. Dotto, A. Zinzi, V. Della Corte, and

- T.S. Statler, "Momentum transfer from the DART mission kinetic impact on asteroid Dimorphos," *Nature*, vol. 616, no. 7957, pp. 457-460, April 2023.
- [3] R.T. Daly, C.M. Ernst, O.S. Barnouin, N.L. Chabot, A.S. Rivkin, A.F. Cheng, E.Y. Adams, H.F. Agrusa, E.D. Abel, A.L. Alford, and E.I. Asphaug, "Successful kinetic impact into an asteroid for planetary defence," *Nature*, vol. 616, no. 7957, pp. 443-447, April 2023.
- [4] S.D. Raducan, M. Jutzi, A.F. Cheng, Y. Zhang, O. Barnouin, G.S. Collins, R.T. Daly, T.M. Davison, C.M. Ernst, T.L. Farnham, and F. Ferrari, "Physical properties of asteroid Dimorphos as derived from the DART impact," *Nature Astronomy*, pp. 1-11, February 2024.
- [4] NASA, URL: <https://www.jpl.nasa.gov/news/nasa-study-asteroids-orbit-shape-changed-after-dart-impact> (Assessed on 14 April 2024).
- [6] S.P. Naidu, S.R. Chesley, N. Moskovitz, C. Thomas, A.J. Meyer, P. Pravec, P. Scheirich, D. Farnocchia, D.J. Scheere, M. Brozovic, and L.A. Benner, "Orbital and physical characterization of asteroid dimorphos following the DART impact," *The Planetary Science Journal*, vol. 5, no. 3, p. 74, March 2024.
- [7] A.M. Stickle, E.S.G. Rainey, M.B. Syal, J.M. Owen, P. Miller, O.S. Barnouin, C.M. Ernst, S.D. Raducan, M. Jutzi, A.F. Cheng, and AIDA/DART Impact Simulation Working Group, "Modeling impact outcomes for the Double Asteroid Redirection Test (DART) mission," *Procedia Engineering*, vol. 204, pp. 116-123, January 2017.
- [8] D.E. Gault, E.M. Shoemaker, H.J. Moore, "Spray ejected from the lunar surface by meteoroid impact," *NASA Technical Note*, no. 1767, April 1963.
- [9] D. Stoeffler, D.E. Gault, J. Wedekind, and G. Polkowski, "Experimental hypervelocity impact into quartz sand - Distribution and shock metamorphism of ejecta," *J. Geophys. Res.*, vol. 80, pp. 4062-4077, October 1975.
- [10] W.K. Hartmann, "Impact experiments. I - Ejecta velocity distributions and related results from regolith targets," *Icarus*, vol. 63, pp. 69-98, July 1985.
- [11] K.R. Housen, and K.A. Holsapple, "Ejecta from impact craters," *Icarus*, vol. 211, no. 1, pp. 856-75, January 2011.
- [12] K.A. Holsapple and K.R. Housen, "Momentum transfer in asteroid impacts. I. Theory and scaling," *Icarus*, vol. 221, no. 2, pp. 875-887, November 2012.
- [13] M. Jutzi and P. Michel, "Hypervelocity impacts on asteroids and momentum transfer I. Numerical simulations using porous targets," *Icarus*, vol. 229, pp. 247-253, February 2014.
- [14] A.M. Stickle, E.S.G. Rainey, M.B. Syal, J.M. Owen, P. Miller, O.S. Barnouin, C.M. Ernst, and the AIDA Impact Simulation Working Group, "Modeling impact outcomes for the Double Asteroid Redirection Test (DART) mission," *Procedia Engineering*, vol. 204, pp. 116-123, January 2017.
- [15] E.S.G. Rainey, A.M. Stickle, A.F. Cheng, A.S. Rivkin, N.L. Chabot, O.S. Barnouin, C.M. Ernst, and the AIDA/DART Impact Simulation Working Group, "Impact modeling for the Double Asteroid Redirection Test (DART) mission," *International Journal of Impact Engineering*, vol. 142, p. 103528, August 2020.
- [16] W.J. Tedeschi, J.L. Remo, J.F. Schulze, and R.P. Young, "Experimental hypervelocity impact effects on simulated planetesimal materials," *International Journal of Impact Engineering*, vol. 17, no. 4-6, pp. 837-48, January 1995.
- [17] M.B. Syal, J.M. Owen, and P.L. Miller, "Deflection by kinetic impact: Sensitivity to asteroid properties," *Icarus*, vol. 269, pp. 50-61, May 2016.
- [18] A.M. Stickle, M.E. DeCoster, C. Burger, W.K. Caldwell, D. Graninger, K.M. Kumamoto, R. Luther, J. Ormö, S. Raducan, E. Rainey, and C.M. Schäfer, "Effects of impact and target parameters on the results of a kinetic impactor: predictions for the Double Asteroid Redirection Test (DART) mission," *The planetary science journal*, vol. 3, no. 11, p. 248, November 2022.
- [19] R. Luther, S.D. Raducan, C. Burger, K. Wünnemann, M. Jutzi, C.M. Schäfer, D. Koschny, T.M. Davison, G.S. Collins, Y. Zhang, and P. Michel, "Momentum enhancement during kinetic impacts in the low-intermediate-strength regime: benchmarking and validation of impact shock physics codes," *The Planetary Science Journal*, vol. 3, no. 10, p. 227, October 2022.
- [20] F. Ferrari, S.D. Raducan, S. Soldini, and M. Jutzi, "Ejecta formation, early collisional processes, and dynamical evolution after the DART impact on Dimorphos," *The Planetary Science Journal*, vol. 3, no. 7, p. 177, July 2022.
- [21] D. Cotto-Figueroa, E. Asphaug, L.A. Garvie, A. Rai, J. Johnston, L. Borkowski, S. Datta, A.

Chattopadhyay, M.A. Morris, "Scale-dependent measurements of meteorite strength: Implications for asteroid fragmentation," *Icarus*, vol. 277, pp. 73-77, October 2016.

- [22] Y. Yu and P. Michel, "Ejecta cloud from the AIDA space project kinetic impact on the secondary of a binary asteroid: II. Fates and evolutionary dependencies," *Icarus*, vol. 312, pp. 128-144, September 2018.
- [23] S.Y. Ren, Z.Z. Gong, Q. Wu, G.M. Song, Q.M. Zhang, P.L. Zhang, C. Chen, and Y. Cao, "Satellite breakup behaviors and model under the hypervelocity impact and explosion: A review," *Defence Technology*, August 2022.
- [24] S.W. Paek, O. de Weck, J. Hoffman, R. Binzel, and D. Miller, "Optimization and decision-making framework for multi-staged asteroid deflection campaigns under epistemic uncertainties," *Acta Astronautica*, vol. 167, pp. 23-41, February 2020.